Pergamon

Cement and Concrete Research, Vol. 28, No. 2, pp. 271–283, 1998

0008-8846/98 $19.00 + .00

PII S0008-8846(97)00269-X

EFFECT OF FLY ASH AND SILICA FUME ON COMPRESSIVE AND FRACTURE BEHAVIORS OF CONCRETE

L. Lam, Y.L. Wong, and C.S. Poon[1]
Department of Civil and Structural Engineering, The Hong Kong Polytechnic University, Hung Hom Kowloon, Hong Kong

(Received July 14, 1997; in final form December 17, 1997)

ABSTRACT

The effects of replacing cement by fly ash and silica fume on strength, compressive stress-strain relationship, and fracture behavior of concrete were investigated. The investigation covered concrete mixes at different water-cementitious material ratios, which contained low and high volumes of fly ash, and with or without the addition of small amount of silica fume. It was found that fly ash substantially improved the post-peak compressive behavior of concrete, with a relatively smaller gradient in the descending part of the stress-strain curve. Low volumes of fly ash improved the tensile strength of concrete. High volume fly ash concrete showed slightly lower tensile strength, but higher values of crack tip opening displacement and final mid-span deflection in the fracture tests, with the corresponding K_{IC} and G_F values similar to or higher than the plain cement concrete. A small amount of silica fume had a large positive effect on the cylinder compressive strength and tensile strength but less on the cube compressive strength, while the fracture behavior of the resulting concrete was brittle. Improving interfacial bond between the paste and the aggregates in concrete had positive effects on K_{IC}, but did not necessarily produce higher G_F values. © *1998 Elsevier Science Ltd*

Introduction

Fly ash has been commonly used to replace part of cement in concrete, and the percentage of replacement ranges from about 20% (low volume fly ash) to more than 50% (high volume fly ash) of the total mass of cementitious materials. In low volume fly ash concrete, the fly ash acts as a pozzolanic material. In high volume fly ash concrete, only part of the fly ash participates in the pozzolanic reaction; the other part remains unreacted even after a long period of curing (1–5).

Research studies indicated that high volume fly ash cement paste may be considered as a new composite material in which fly ash particles perform as reactive micro-aggregates embedded in a mixture of hydration and reaction products, and crack generally propagates

[1]To whom correspondence should be addressed.

around the fly ash particles (3). Consequently, the compressive stress-strain curve of high volume fly ash paste is less linear than that of plain cement paste (3). It is evident that a high volume of fly ash modifies the microstructure of the cement paste and such modification will also affect the macromechanical behavior of the concrete. Previous studies (6–9) revealed that high volume fly ash concretes generally have higher modulus of elasticity, lower shrinkage and creep, as compared to the Portland cement (PC) concretes having equivalent compressive strength. This is because the unreacted fly ash particles have higher modulus of elasticity than the cement hydration products (3). However, other important properties, such as compressive stress-strain relation and fracture behavior, have not been thoroughly quantified.

This paper aims to present the results of the effect of both low and high volume fly ash replacements on the mechanical and fracture behaviors of concrete. The mechanical and fracture parameters studied included 1) mechanical strength: cube compressive strength (f_c), cylinder compressive strength (f'_c), and tensile splitting strength (f'_{sp}); 2) complete compressive stress-strain relationship; and 3) fracture properties: fracture energy (G_F) based on the Fictitious Model of Hillerborg et al. (10,11), critical stress intensity factor (K_{IC}) and critical crack tip opening displacement ($CTOD_C$) based on the Two-parameters model of Jenq and Shah (12). As the combined use of fly ash and a relative small amount of silica fume is common in the concrete industry (13), the influence of adding silica fume is also included in this study.

Experimental Details

Mix Details and Specimen Preparation

The experimental work covered three series of concrete mixes with water-cementitious material ratios (W/CM) of 0.3 (S1), 0.4 (S2), and 0.5 (S3), respectively. The cementitious materials were Portland cement equivalent to ASTM Type I, low calcium fly ash equivalent to ASTM Class F, and a condensed silica fume commercially available in Hong Kong. In each mix series, the levels of cement replacement by fly ash (on direct weight to weight basis) varied from 0 to 55%. In some mixes, a further 5% silica fume replacement was made. The coarse aggregates were crushed granites, with a maximum size of 10 mm for mixes with W/CM of 0.3, and 20 mm for mixes with W/CM of 0.4 and 0.5. A smaller size of coarse aggregate was used for the mixes with lower W/CM because of the consideration of workability. River sand was used as fine aggregates. A naphthalene-based high range water reducing admixture (HRWRA) was used in mixes at W/CM of 0.3 and 0.4 to achieve workability with slump not less than 75 mm. Air entraining admixture was not applied. Table 1 lists the details of the concrete mixes.

Cubes (100 mm in size) were prepared for the determination of f_c, and cylinders (100 mm dia. $\times$ 200 mm) were prepared for the determination of complete compressive stress-strain curves, f'_c and f'_{sp}. Beams (350 mm $\times$ 75 mm $\times$ 50 mm ($L \times b \times d$)) with a 25-mm deep notch at mid-span were cast for the fracture tests. All specimens were cured in water at 27°C according to Hong Kong practice. The cube compressive strength was measured at 3, 7, 28, 90, and 180 days. Other tests were carried out at 28 and 56 days. The number of specimens prepared for each test was three for cube compressive strength and fracture properties, and

TABLE 1
Details of concrete mixes.

				Mix proportion, kg/m^3				
Mix	W/CM	Fly ash, %	Silica fume, %	Total cementitious materials	Fine aggregate	Coarse aggregate	Water	HRWRA, L/m^3
S1-0-0	0.3	0	0	500	724	1086	150	7.5
S1-15-0	0.3	15	0	500	700	1086	150	7.5
S1-25-0	0.3	25	0	500	683	1086	150	9.25
S1-45-0	0.3	45	0	500	650	1086	150	10.5
S1-55-0	0.3	55	0	500	634	1086	150	13.0
S1-0-5	0.3	0	5	500	719	1086	150	8.0
S1-20-5	0.3	20	5	500	686	1086	150	9.25
S1-40-5	0.3	40	5	500	654	1086	150	11.0
S2-0-0	0.4	0	0	400	710	1157	160	4
S2-15-0	0.4	15	0	400	690	1157	160	4.4
S2-25-0	0.4	25	0	400	660	1157	160	4.8
S2-45-0	0.4	45	0	400	634	1157	160	5.2
S2-55-0	0.4	55	0	400	621	1157	160	6.4
S2-0-5	0.4	0	5	400	688	1157	160	5.5
S2-20-5	0.4	20	5	400	662	1157	160	5.5
S2-40-5	0.4	40	5	400	636	1157	160	6
S3-0-0	0.5	0	0	410	609	1132	205	0
S3-15-0	0.5	15	0	410	589	1132	205	0
S3-25-0	0.5	25	0	410	576	1132	205	0
S3-45-0	0.5	45	0	410	549	1132	205	0
S3-55-0	0.5	55	0	410	536	1132	205	0
S3-0-5	0.5	0	5	410	605	1132	205	0
S3-20-5	0.5	20	5	410	578	1132	205	0
S3-40-5	0.5	40	5	410	552	1132	205	0

two for cylinder compressive strength, tensile splitting strength, and complete compressive stress-strain curves.

Testing Procedures

Compressive strengths of the cubes and cylinders were determined with a loading rate of 0.33 N/mm^2 per second. Tensile splitting strength was determined using a loading rate of 0.03 N/mm^2 per second. The complete stress-strain curves in compression were obtained by applying the load on the cylinders at a constant axial displacement rate of 0.1 mm/min.

The fracture parameters G_F, K_{IC}, and $CTOD_C$ were determined according to RILEM recommendations (14,15) by means of three-point bending tests on notched beams, using a closed loop servo-controlled MTS testing system. The specimen size was smaller than the standard size so that it could fit to available equipment (Fig. 1). A crack opening displacement (COD) gauge, held by two knife edges that were glued on the downward surface of both

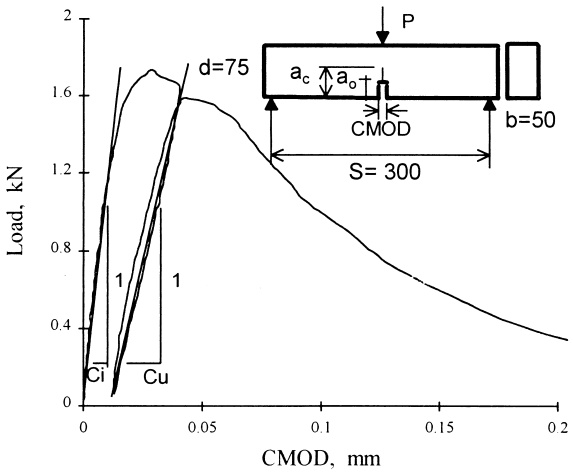

FIG. 1.
Schematic illustration of the fracture tests.

sides of the notch mouth of the beam, was used to measure the crack mouth opening displacement (CMOD).

The net mid-span deflection of the beam was measured by means of two linear variable displacement transducers (LVDT). Load was applied to the beams at a constant CMOD rate (0.0002 mm/s). An unloading-reloading cycle was performed when the load decreased in the post-peak area to about 95% of the maximum load. Thereafter application of the load was continued until the beam was broken (see Fig. 1). The fracture energy G_F was calculated from the area under the load-deflection curve. The calculations of K_{IC} and $CTOD_C$ were based on the maximum load, and the initial and unloading compliances. Further details of the calculations are shown in the Appendix of this paper.

Results and Discussion

Compressive Strength and Tensile Splitting Strength

As shown in Table 2 and Figure 2, fly ash contributed little to strength at early ages. At 3 days, compared to the PC concrete the cube compressive strength was reduced by 16% in average for a 15% fly ash replacement, and by 66% for a 55% fly ash replacement. At 28 days, the strength of the 15% fly ash mixes was only slightly lower (4% in average) than the PC mixes, although 55% fly ash replacement still resulted in a 44% strength reduction. At the later ages, the contribution of fly ash to compressive strength became larger. These observations are consistent with the results of other studies (16,17). The contribution of fly ash in concrete mixes prepared at a lower W/CM was greater than those prepared at a higher W/CM. For instance, at 56 days, the 55% fly ash mix at W/CM 0.3 achieved 77% of the cylinder compressive strength of the reference PC mix, but the corresponding mixes at the W/CM of 0.4 and 0.5 achieved only 64% and 66% respectively of the strength of the reference PC mixes.

TABLE 2
Compressive strength and tensile splitting strength test results.

Age, days	Compressive strength, MPa								Tensile splitting strength, MPa	
	f_c						f'_c		f'_{sp}	
	3	7	28	56	90	180	28	56	28	56
S1-0-0	64.9	75.5	86.8	87.2	95.7	97.7	82.5	86.5	5.27	5.52
S1-15-0	52.1	66.4	86.0	94.8	99.6	106.3	77.9	89.5	5.45	5.91
S1-25-0	48.0	65.7	85.4	90.4	95.4	107.8	79.1	86.5	5.23	5.75
S1-45-0	34.1	49.2	71.8	85.4	87.7	97.7	64.0	77.3	4.51	5.23
S1-55-0	22.3	36.4	57.4	66.6	72.8	79.9	57.1	66.9	3.13	4.55
S1-0-5	58.3	75.5	87.8	93.1	93.6	99.3	87.7	92.3	5.76	5.86
S1-20-5	46.3	65.6	78.5	85.8	90.3	95.9	84.2	86.5	5.70	5.79
S1-40-5	30.5	48.6	71.1	80.0	83.4	88.3	71.6	76.1	4.90	5.47
S2-0-0	35.0	48.4	60.7	67.1	70.5	70.6	55.8	58.6	3.93	3.94
S2-15-0	29.3	39.9	56.0	63.4	68.5	72.1	44.8	49.4	3.75	4.58
S2-25-0	24.7	33.7	49.3	60.8	66.2	70.2	44.1	53.6	3.91	4.37
S2-45-0	14.5	20.3	43.9	54.1	61.2	63.7	32.7	42.1	2.91	3.51
S2-55-0	13.6	19.8	37.3	47.1	52.9	63.2	32.4	37.7	2.97	3.43
S2-0-5	37.3	53.0	69.4	72.1	73.7	74.5	64.8	64.8	4.57	5.07
S2-20-5	28.9	42.1	62.3	69.9	72.4	76.0	56.2	61.7	4.39	4.62
S2-40-5	14.5	20.5	44.6	55.3	59.1	68.4	40.5	47.3	3.36	3.37
S3-0-0	26.1	36.9	50.8	57.1	58.1	60.6	42.6	45.8	3.66	4.02
S3-15-0	23.3	32.3	48.9	55.7	62.6	64.8	38.1	46.7	3.53	3.92
S3-25-0	18.4	26.2	41.7	49.1	53.7	57.9	35.2	43.6	3.09	3.26
S3-45-0	13.4	18.4	35.6	47.0	54.1	56.6	30.4	37.6	2.79	3.16
S3-55-0	7.8	11.3	24.0	33.7	41.4	48.3	25.9	30.4	2.32	3.16
S3-0-5	27.4	39.2	57.3	59.6	67.3	66.3	46.8	54.2	3.97	4.05
S3-20-5	20.1	30.6	52.9	60.7	63.7	68.0	46.8	53.1	3.89	4.08
S3-40-5	11.4	16.8	38.7	45.9	48.7	58.4	33.2	37.4	3.28	3.83

It can also be noted that the enhancement effect of 5% silica fume on the cube compressive strength was not as significant as on the cylinder compressive strength and tensile splitting strength. The results showed about 17% increase for f'_c and 13% increase for f'_{sp}, but only 7% increase for f_c (see strength values of the mixes containing 5% silica fume, e.g., S1-0-5, S1-20-5, and the mixes without silica fume, e.g., S1-0-0, S1-25-0). The higher tensile strength and cylinder compressive strength of the silica fume concretes can be attributed to the improved interfacial bond between the paste and the aggregate (18). It is believed that the improvement of the interfacial bond is less effective on enhancing cube compressive strength than on cylinder compressive strength, because the cube specimens have a lower height to width ratio as compared with cylinder specimens, and are more influenced by the end restrain effects.

Fly ash may also improve the interfacial bond. In Figure 3, the 28- and 56-day tensile splitting strength values (f'_{sp}) of the different mixes are plotted against the squared root of

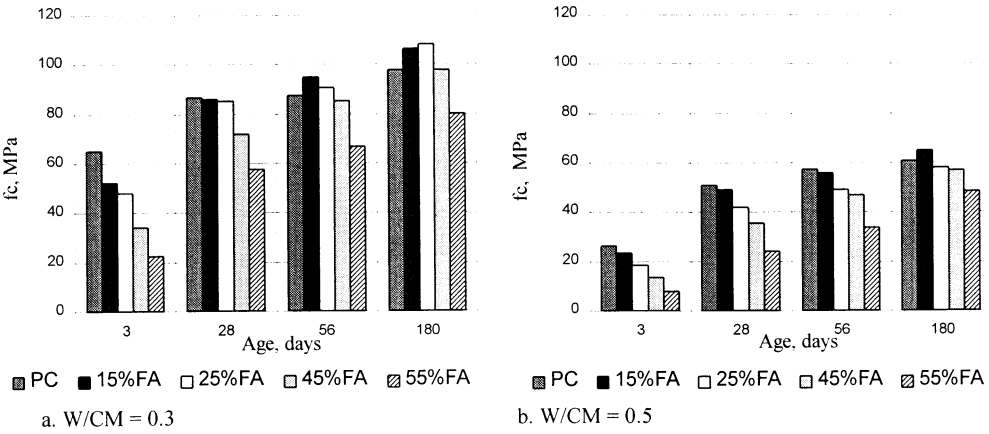

FIG. 2.
Effects of fly ash replacement on cube compressive strength (f_c) development.

their cylinder compressive strength values (214 f'_c). In the literature (19), it is generally accepted that f'_{sp} and 214 f'_c have a linear relationship. But in Figure 3, there is a trend that at equivalent compressive strength level, the mixes containing 15–25% fly ash or 5% silica fume have higher tensile splitting strength values than the plain cement (PC) mixes. This trend becomes more significant when the compressive strength level increases. For instance, at the compressive strength level of 80 MPa, the f'_{sp} of the mixes with 15 to 25% fly ash or 5% silica fume may be 7% higher than the PC mixes. This indicates that proper amounts of fly ash replacement may have positive effects on the interfacial bond between the paste and the aggregates. The mixes containing 45–55% fly ash showed lower tensile strength, probably due to the lower concentration of cement hydration products, as interfacial bond development in high volume fly ash concrete requires a longer period of curing.

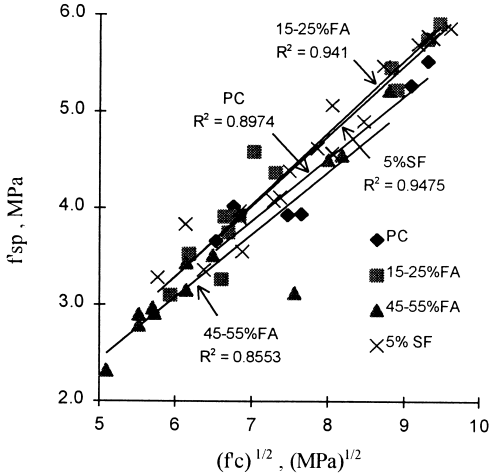

FIG. 3.
Effects of fly ash and silica fume on tensile splitting strength (at 28 days and 56 days) reference PC mixes.

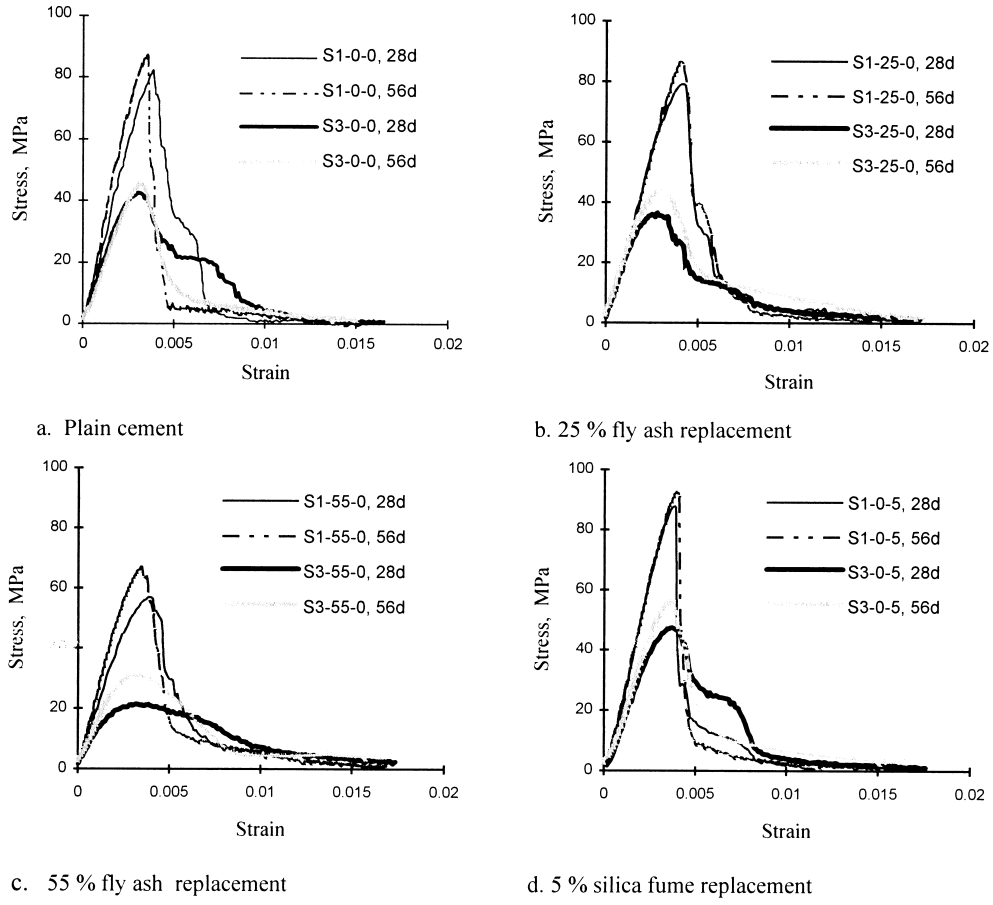

FIG. 4.
Complete compressive stress-strain curves of concrete mixes with different cementitious constituents.

Complete Stress-Strain Relationship in Compression

Complete compressive stress-strain curves of concrete mixes with different cementitious constituents at 28 and 56 days are shown in Figures 4a–d. It should be noted that the strain values used to construct these curves were obtained from the full height displacement of cylinders. Other approaches, such as strain gauges or LVDTs set on the specimen surface, by which the strain values at the mid-height of the specimen are measured, were not used because of the spalling of the concrete surface at failure making measurement of the final strain values difficult. For the ascending parts of the curves, such values might be about 30% higher than those values measured at the middle height of the cylinders. In design codes such as the CEB-FIP 1990 Model Code (MC90) (20), compressive stress-strain relationships of concrete are usually considered to be dependent on concrete strength. However, the stress-strain curves shown in Figure 4 indicate that the nature of cementitious constituents is also important. In comparison, the curves of fly ash concretes are broader and have smaller

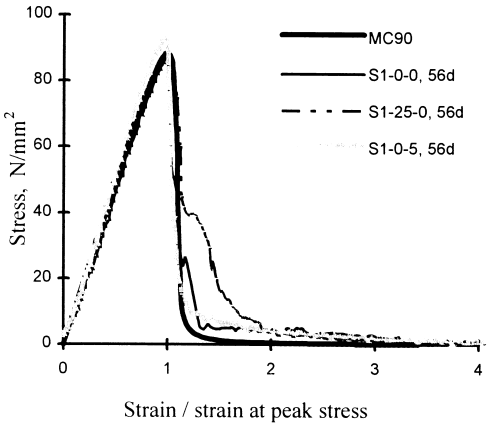

FIG. 5.
Comparison of normalized stress-strain curves of plain cement, fly ash, and silica fume concretes (at 56 days) with standard MC90 curve.

gradients in the descending parts, but the curves of PC and silica fume concrete mixes are sharper, and have more rapid descending paths. A comparison of the measured stress-strain curves with the design stress-strain curve recommended by MC90 (20) is illustrated in Figure 5, where all curves are normalized and the peak stress value taken for the MC90 curve is the average f'_c of the three mixes (S1-0-0, S1-25-0, and S1-0-5). It is observed that, the curves of PC and silica fume concrete mixes approximately fit the MC90 curve, but the curve of fly ash concrete (S1-25-0) obviously deviates from the MC90 curve. The total area under the curve of the fly ash concrete is about 12% larger than that of the PC concrete and 16% larger than that of the silica fume concrete. Further comparing of the results of other mixes with the MC90 expressions can have similar observation. These observations suggested that replacement of cement by fly ash improves the post-peak compressive behavior of concrete.

Figure 6 shows that the measured strain values at peak stress (ϵ_{cl}) substantially increased with compressive strength, and for a given compressive strength, increasing fly ash replacement in concrete tended to increase values of ϵ_{cl} (maximum increase in ϵ_{cl} values can be

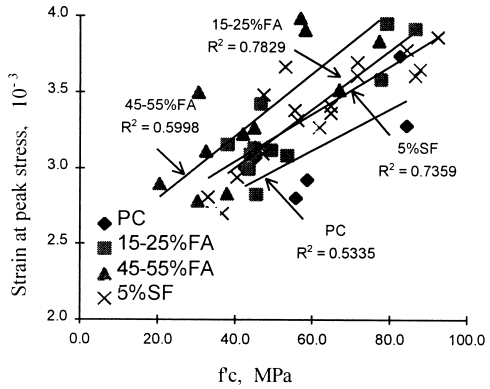

FIG. 6.
Effects of fly ash, silica fume on strain at peak stress in compression.

TABLE 3
Summarized results of fracture tests.

	P_{max}, kN	Critical crack length (a_c), mm	K_{IC}, MPa$\sqrt{m}$	$CTOD_C$, 10^{-2} mm	Final mid span deflection (δ_o), mm	G_F, N/m
			28 days			
S1-0-0	1.80	35.0	1.19	1.39	0.54	114.8
S1-25-0	1.78	33.8	1.19	1.11	0.68	120.5
S1-45-0	1.71	34.2	1.18	1.25	0.79	123.5
S1-55-0	1.48	38.3	1.19	1.84	1.34	122.2
S1-0-5	2.08	30.9	1.23	1.15	0.64	111.6
			56 days			
S1-0-0	1.93	32.8	1.23	1.31	0.67	123.3
S1-25-0	1.97	28.0	1.25	1.30	0.65	121.5
S1-45-0	2.12	32.9	1.36	1.26	0.72	126.4
S1-55-0	1.6	37.1	1.59	1.52	0.9	120.6
S1-0-5	2.16	28.3	1.21	0.76	0.46	100.4

about 40%). But in design codes (20,21), ϵ_{cl} is usually taken to be a constant values for all mixes.

Fracture Properties (K_{IC}, $CTOD_C$, and G_F)

It has been reported that the critical stress intensity factor (K_{IC}) and fracture energy (G_F) of concrete increase with concrete strength, aggregate size, and content (22–24). High strength concretes containing silica fume are more brittle (22), and the addition of clay improves the fracture toughness of concrete (25). However, the effects of replacing cement by fly ash on the fracture properties of concrete are not known.

As indicated in Table 3 and Figure 7, an increase of fly ash replacement reduced f'_c but

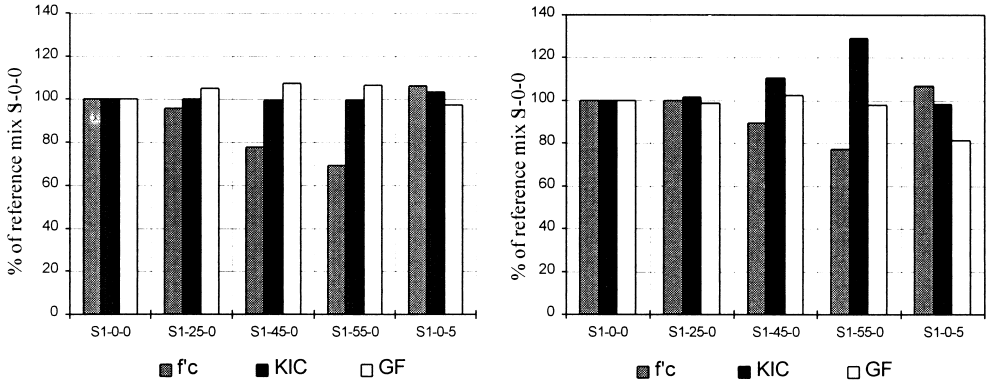

a. at 28 days b. at 56 days

FIG. 7.
Comparison of f'_c, K_{IC}, and G_F (at 28 days and 56 days) of plain cement, fly ash, and silica fume concretes.

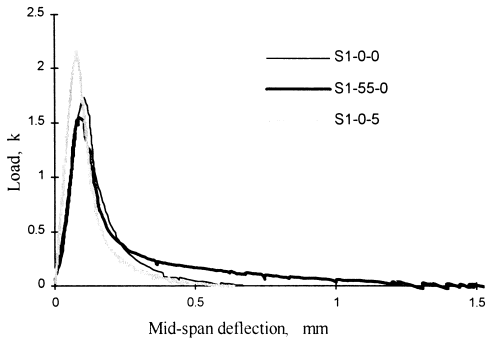

FIG. 8.
Fracture behavior of plain cement, silica fume, and high volume fly ash concretes (at 28 days).

improved the fracture properties K_{IC} and $CTOD_C$. When compared with the test results of the reference mix S1-0-0, the specimens made with 45% and 55% fly ash replacements exhibited slightly lower load bearing capacity (P_{max}), but larger crack tip opening displacement ($CTOD_C$) and final mid span deflection (δ_o), giving similar or higher values of K_{IC} and G_F. It can also be noticed that from the ages of 28 days to 56 days, the high volume fly ash mixes had about 30% increase in K_{IC} but about 15% decrease in final mid-span deflection (δ_o). On the contrary, the mix containing 5% silica fume had higher compressive strength (f'_c) and load bearing capacities (P_{max}), equal or higher values of K_{IC}, but lower values of $CTOD_C$ and fracture energy (G_F).

Figure 8 shows the load-deflection curves of PC, silica fume, and high volume fly ash concrete specimens in the fracture test. Clearly, as revealed by the differences in the values of mid-span deflection recorded, high volume fly ash specimens are tougher than the others, with larger displacement before fracture.

The above results reveal that replacing cement by high volume fly ash has beneficial effects on the fracture properties of concrete. This can be explained based on Zhang's model (3) for high volume fly ash cement paste. According to this model, high volume fly ash cement paste can be considered as a multiphase composite material. The unreacted fly ash particles in the paste may act as micro-aggregates with higher modulus of elasticity, which increase the resistance to crack propagation. Also, cracking around the fly ash particles results in more energy to be dissipated before failure. With these features, the fracture process of high volume fly ash concrete becomes less linear and the material becomes tougher. This explanation can also be applied to the compressive behavior of high volume fly ash concrete.

The results also show that the fracture parameters K_{IC} and G_F have different responses to material characteristics. In many cases, these two parameters do not simultaneously increase or decrease. For the mix with 5% silica fume, the K_{IC} values were comparable with other mixes, but the G_F values were smaller. For high volume fly ash mixes, with increasing curing age, the K_{IC} values increased but the G_F value remained unchanged. The above observations are related to the paste-aggregate interfacial bond and the microstructural heterogeneity in the concrete. It is generally believed that the enhanced interfacial bond is responsible for the brittleness of silica fume concretes (22), and renders the microstructure of the silica fume concrete more homogeneous (26). This leads to a rapid propagation of crack after the peak load is reached and hence lower G_F values. For fly ash concrete, it has been shown that at

early ages, only low volumes of fly ash may have a beneficial effect on the interfacial bond, while the interfacial bond development of high volume fly ash concrete requires longer period of curing. Therefore, as K_{IC} represents a local toughness parameter, and is largely dependent on the tensile property of concrete, prolonged curing has a positive effect on K_{IC} for high volume fly ash concrete. On the other hand, as G_F is considered as a material constant determined by a more complex phenomenon of the fracture process zone (27), improving K_{IC} in high volume fly ash concrete does not necessarily produce higher G_F values.

Conclusions

1. A 15 to 25% fly ash replacement had beneficial effect on the tensile strength of concrete. Higher volumes of fly ash replacement resulted in slightly lower tensile strength at the ages of 28 day and 56 days. A 5% silica fume replacement had a significant positive effect on the cylinder compressive strength and tensile splitting strength, but less on the cube compressive strength.
2. Incorporating fly ash improved the post-peak compressive behavior of concrete, with a lower gradient in the descending part of the stress-strain curve. Fly ash also increased the strain values at peak stresses.
3. Replacing cement by high volumes of fly ash improved the fracture properties of concrete. A 45% to 55% fly ash replacement resulted in slightly lower load bearing capacity, but larger crack tip opening displacement ($CTOD_C$) and final mid-span deflection (δ_o), giving the K_{IC} and G_F values similar to or higher than the plain cement concrete.
4. The effect of a small amount of silica fume on the cube compressive strength is not as significant as on the cylinder compressive strength. The compressive and fracture behaviors of silica fume concrete are more brittle than plain cement concrete.
5. Improving interfacial bond between the paste and the aggregate has positive effect on K_{IC}, but does not necessarily produce higher values of G_F.
6. In the light of the results of this study, the appropriateness of common design practice treating the mechanical and fracture properties of all concretes as functions of its compressive strength only, regardless of the constitution of cementitious materials should be reconsidered. In case of high volume fly ash concrete, the enhancing effect of fly ash on the fracture properties of concrete should be thoroughly quantified and if possible incorporated in the future concrete design codes.

References

1. CUR Report 144, research carried out by INTRON, Fly Ash Addition to Concrete. A.A. Balkama, Rotterdam, 1992.
2. E.E. Berry, R.T. Hemmings, and B.J. Cornelins, Cem. Concr. Compos. 12, 253 (1990).
3. M.H. Zhang, Cem. Concr. Res. 25, 1165 (1995).
4. R.F. Feldman, G.G. Carette, and V.M. Malhotra, Cem. Concr. Compos. 12, 245 (1990).
5. E.E. Berry, R.T. Hemmings, M.H. Zhang, B.J. Cornelins, and D.M. Golden, ACI Mater. J. 91, 382 (1994).
6. V.M. Malhotra, Concr. Int. 8, 28 (1986).
7. W.S. Langley, C.G. Carette, and V.M. Malhotra, ACI Mater. J. 86, 507 (1989).

8. V. Sivasundaram, G.G. Carette, and V.M. Malhotra, Cem. Concr. Compos. 12, 263 (1990).
9. V. Sivasundardam, G.G. Carette, and V.M. Malhotra, ACI Mater. J. 88, 407 (1991).
10. A. Hillerborg, M. Modeer, and P-E Petersson, Cem. Concr. Res. 6, 773 (1976).
11. A. Hillerborg, Fracture Mechanics of Concrete, F.H. Wittman (ed.), p. 223, Elsevier, Amsterdam, 1983.
12. Y. Jenq and S.P. Shah, J. Engng. Mech. ASCE 1, 1227 (1985).
13. C. Ozylidirim and W.J. Halsfead, ACI Mater. J. 91, 587 (1994).
14. RILEM 50–FMC Committee, Mater. Struct. 18, 285 (1985).
15. RILEM Committee on Fracture Mechanics of Concrete, Test Methods, using three bend tests. Mater. Struct. 23, 457 (1990).
16. J. Bijen, R.V. Selst, Cem. Concr. Res. 23, 1029 (1993).
17. K.G. Babu and S.N. Bao, Cem. Concr. Res. 26, 465 (1996).
18. A. Goldman and A. Bentur, ACI Mater. J. 86, 440 (1989).
19. ACI Committee 363, State-of-Art Report on High Strength Concrete (ACI363R-92), American Concrete Institute, Detroit, 1992.
20. CEB-FIP Model Code 1990, p. 33. Thomas Telford, London, 1993.
21. ACI-318–89 (Revised 1992), Building Code Requirements for Reinforced Concrete, American Concrete Institute, Detroit, 1992.
22. C. Tasdemir, M.A. Tasdemir, F.D. Lydon, and B.I.G. Barr, Cem. Concr. Res. 26, 63 (1996).
23. R. John and S.P. Shah, J. Mater. Civil Engng. ASCE 1, 185 (1989).
24. F.P. Zhou, B.I.G. Barr, and F.D. Lydon, Cem. Concr. Res. 25, 543 (1995).
25. M. Moukwa, B.G. Lewis, S.P. Shah, and C. Ouyang, Cem. Concr. Res. 23, 711 (1993).
26. K. Vivekanandam and I. Patnaikuni, Cem. Concr. Res. 27, 817 (1997).
27. A. Carpinter and B. Chiaia, Mater. Struct. 29, 259 (1996).

Appendix: Calculations of G_F, K_{IC}, and $CTOD_C$

According to reference (14), the fracture energy G_F is given by:

$$G_F = (w_o + mg\delta_o)/A_{lig} \quad (N/m)$$

where w_o is the area under the load-deflection curve, m, g, δ_o, and A_{lig} are the mass of the beam, acceleration due to gravity, mid-span deflection of the beam at failure, and the section area of the ligament of the beam, respectively.

Referring to reference (15), the fracture property of concrete is described by two parameters, K_{IC} and $CTOD_C$. At first, the Young's modulus is calculated by the initial notch depth a_o and the initial compliance C_i (see Fig. 1). Then the Young's modulus is expressed as:

$$E = 6Sa_oV_1(\alpha)/(C_id^2b) \quad (Nm^{-2})$$

where S, b, and d are span, thickness, and beam depth, respectively. V_1 is a geometrical function of the ratio $\alpha = (a_o + H_o)/(d + H_o)$, H_o = thickness of the knife edges. For $S/d = 4$, $V_1(\alpha) = 0.76 - 2.28\alpha + 3.87\alpha^2 - 2.04\alpha^3 + 0.66/(1 - \alpha)^2$.

The critical crack length a_c is determined by iteration from $a_c = EC_ubd^2/[6SV_1(\alpha_1)]$, where C_u is the unloading compliance (Fig. 1) and $\alpha_1 = (a_c + H_o)/(d + H_o)$.

The critical stress intensity factor K_{IC} is given by:

$$K_{IC} = 3(P_{max} + 0.5w_oS/L)S(\pi a_c)^{1/2}F(\alpha_2)/2d^2b \quad (10^{-6}\ MPa\sqrt{m})$$

in which $F(\alpha_2) = [1.99 - \alpha_2 (1 - \alpha_2)(2.15 - 3.93\alpha_2 + 2.7\alpha_2^2)]/[\pi^{1/2}(1 + 2\alpha_2)(1 - \alpha_2)^{3/2}]$, where w_o and L are the weight and length of beam, respectively, $\alpha_2 = a_c/d$, and P_{max} = the measured maximum load.

Finally, the critical crack tip opening displacement ($CTOD_C$) is given by:

$$CTOD_C = 6P_{max}Sa_cV_1(\alpha_2)[(1\text{-}\beta)^2 + (1.081 - 1.149\alpha_2)(\beta\text{-}\beta^2)]^{1/2}/Ed^2b \quad \text{(m)}$$

in which $\alpha_2 = a_c/d$ and $\beta = a_o/a_c$.